Application of Surface Sound Speed Measurements in Post-processing for Multi-Sector Multibeam Echosounders

By J.D. Beaudoin and J.E. Hughes Clarke, Ocean Mapping Group (OMG), University of New Brunswick and J.E. Bartlett, Canadian Hydrographic Service, Canada

Abstract

Given sufficient data from ancillary sensors, swath sonar systems can generate sounding solutions in real time. The absolute accuracy of these solutions depends both on the sonar-relative range and angle determination, and particularly on the quality of the aiding information. In this paper, we examine the correction of imperfect surface sound speed information for a multi-sector swath sonar. Difficulties arise from: (1) sector timings and boundaries changing with operational mode, and (2) insufficient information to determine the transmit sector associated with a receive beam. A number of post-processing strategies are proposed and the specific steps in implementation are described in detail.

Résumé

Avec suffisamment d'informations à l'appui, les systèmes de sonar à balayage latéral peuvent générer des solutions de sondage en temps réel. L'exactitude absolue de ces solutions dépend à la fois de la portée relative du sonar et de la détermination de l'angle, et notamment de la qualité des informations fournies. Dans le présent article, nous examinons la correction d'informations imparfaites sur la vitesse du son en surface pour un sonar surfacique à canaux multiples. Les difficultés proviennent des points suivants: (1) modification des temps et limites de secteurs en fonction du mode opérationnel, et (2) informations insuffisantes pour déterminer le secteur émetteur associé au faisceau récepteur. Un certain nombre de stratégies de post-traitement sont proposées et les mesures de mise en œuvre spécifiques sont décrites en détail.

Resumen

Con suficiente información de ayuda, la banda de sistemas sonar puede generar soluciones de sondajes en tiempo real. La precisión absoluta de estas soluciones depende de ambas cosas, la gama relativa al sonar y la determinación de ángulos, y particularmente de la calidad de la información de ayuda. En este artículo examinamos la corrección de información sobre la velocidad del sonido en una superficie imperfecta para sonares de banda multi-sector. Las dificultades vienen de: (1) los ritmos y límites de los sectores que cambian con el modo operativo y (2) de una información insuficiente para determinar el sector de transmisión asociado a un haz de recepción. Se proponen un número de estrategias de posprocesado y se describen de forma detallada las etapas específicas en su implementación.

Introduction

The accuracy of a multibeam survey depends directly on our knowledge of the sound speed, both at the transducer face and throughout the water-column. Uncertainties in either case lead directly to systematic errors in the depth and positioning of soundings. In the ideal situation, both quantities are measured with sufficient temporal and spatial resolution such that their effects are adequately accounted for. This is not always the case, however, and the hydrographer may need to apply new sound speed information in post-processing. This involves re-pointing the beam launch vector given new surface sound speed information and/or re-raytracing using new sound speed profile information. During an autumn transit of the Northwest Passage in 2003, the CCGS *Amundsen* collected swath bathymetry throughout the Passage and also during oceanographic mooring operations in the Beaufort Sea (refer to Figure 1). Lack of sound speed profile collection and failure of the surface sound speed probe led to an extensive amount of post-processing to minimise systematic biases due to sound speed errors. It is the intent of this paper to document the approach taken for the application

of surface sound speed in post-processing for the *Amundsen*'s EM300 (sound speed profile post-processing is discussed by Beaudoin (2004)).

The CCGS *Amundsen* (formerly *Sir John Franklin*) is a 98-metre 1200 class icebreaker completely rigged for various scientific activities and capable of extended stays in the Arctic. The vessel is equipped with a Kongsberg-Simrad EM300, which is a shallow to mid ocean depth system (nominally 10m - 5,000m) with a nominal frequency of 30kHz. The transmit fan is split into several frequency-coded sectors ranging from 27 -34kHz, with the number of sectors varying from three to nine depending on the operating mode (which is depth dependant). These sectors are transmitted sequentially at each ping which leads to complications during the determination of vessel orientation at transmit and receive times, as will be discussed later.

The vessel was equipped with a hull-mounted sound speed probe that provided real-time transducer surface sound speed to the transceiver to ensure correct beam steering. For sound speed throughout the water column, the vessel was equipped with a Brooke Ocean Technology MVP-300 (Moving Vessel Profiler) that was capable of being towed behind the vessel, collecting water column information along the vessel track through a repetitive freefall dipping motion. In the ideal situation, the sensor would be deployed at all times during a survey and the water column information applied immediately.

The reality of the first transit operations was that the crew was concerned for the safety of the MVP system, this concern being aggravated by the intermittent ice cover throughout the Passage. A secondary issue became a critical factor however: as the system was fitted with a
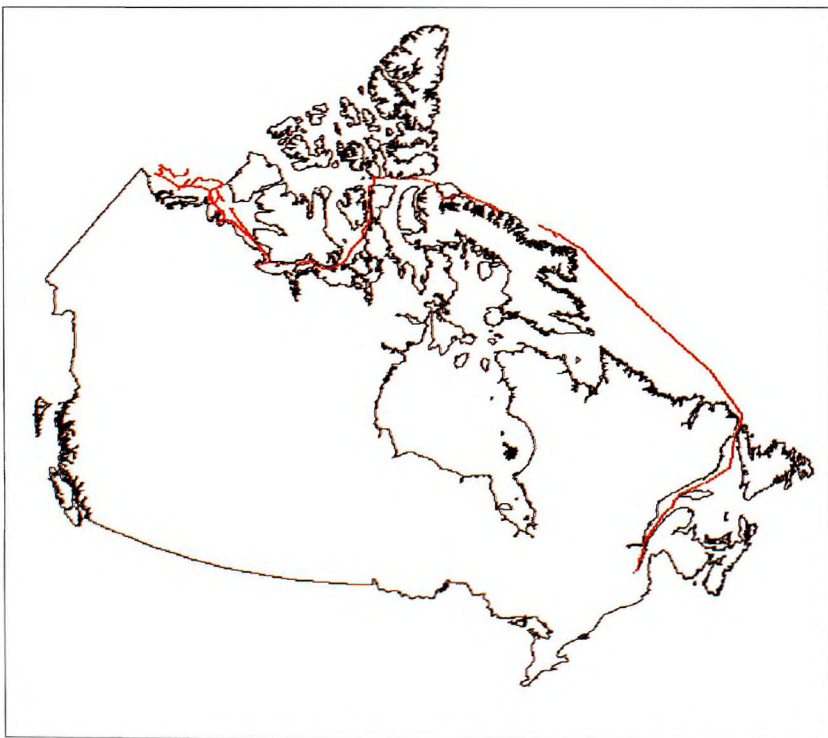

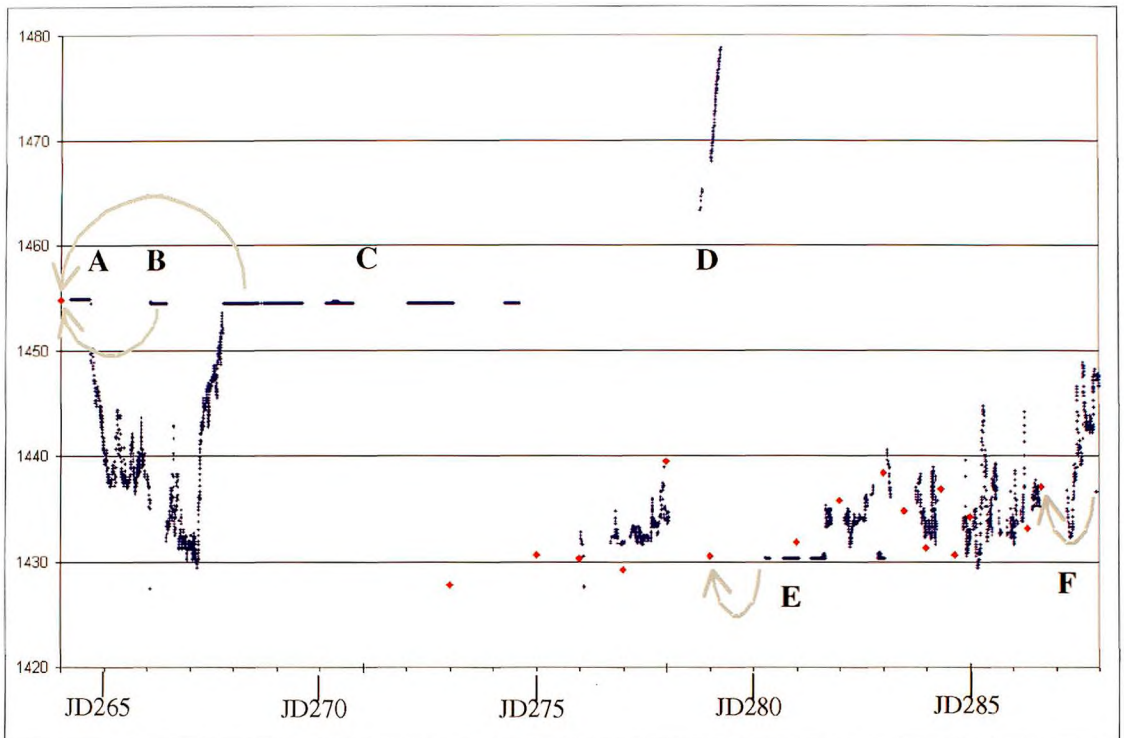*Figure 1: Ship track of CCGS Amundsen, September 2003, departing from Quebec City.*

Figure 2: Time-series plot of surface sound speed measured throughout the cruise. Red points signify sound speed measured from a sound speed profile, blue points represent the sound speed used by the transceiver in beam steering calculations; this value is either taken from a real-time probe on the hull or from the last sound speed profile (or from an operator specified value, though this option was never exercised). Time-axis is labeled in Julian days; vertical axis is sound speed in metres per second.

glass conductivity cell (part of a Seabird 911 CTD), it could not be allowed to fill with the fresh water commonly found at the sea surface otherwise it would freeze and destroy the sensor. This limited the use of underway MVP operations, as such the only sound speed profiles were obtained when a CTD rosette cast was performed at the location of an oceanographic mooring deployment. This yielded only 16 profiles over the course of a 25-day survey. In addition to the lack of sound speed profiles, the pump that supplied the surface sound speed probe would occasionally fail. Until the operator noticed the failure, the water in the probe would heat to inner hull temperatures and artificially raise the sound speed.

Plots of the surface sound speed used in beam steering calculations have been prepared and are shown in Figure 2. Several artifacts can be noted in the raw data; for example, Section D demonstrates the effect of an unnoticed (or overnight) pump failure with a steady rise in sound speed until the failure was noticed. While the sound speed probe was being repaired, the operator chose to use the sound speed from the last collected sound profile as an approximation of the true surface sound speed (as shown by the grey arrows in Figure 2), leading to the flat-line sound speed observations in E. Similar flat line events occur in A, B, C, and F. In all five cases, the sound speed used for beam steering was taken from the last sound profile and the surface sound speed probe data were ignored (whether the data were acceptable or not).

Post-processing Methodology

Overview of Methodology

Faced with erroneous surface sound speed values, incorrect soundings may be corrected based on an estimate of the correct surface sound speed as long as the following data are preserved in the raw data stream [Hughes Clarke, et al. 2000]:

1. Array relative steering angles

Surface Sound Speed	Sound Speed Profile	Entry Point
New value	New profile	Step 1
New value	Acceptable profile	Step 1
Acceptable value	New profile	Step 3

Table 1: Application of new sound speed information for an electronically steered array.

2. Two way travel times (twtt) to bottom detection point
3. Full resolution orientation time series
4. Lever arms between all sensors, and alignment angles
5. Sound speed applied in beam steering process.

In the general case, one must begin with the fundamental measurements made by the sonar, i.e. twtt and angle, and re-point the original array-relative steering angles if necessary (beam pointing angle in Figure 3). The next step is to recreate the sounding geometry at transmit and receive in order to determine the beam's geographic launch vector (beam launch angle in Figure 3). Having done this, an acoustic ray trace provides the depth and horizontal range with the beam azimuth being used to reduce the horizontal measurement into across-track and along-track components. Finally, the lever arms between the reference point and the transducer are rotated using the transmit orientation, and are then added to the depth, across-track and along-track offsets to yield the sounding solution with respect to the reference point. The above boils down to a four-step process:

1. Re-compute beam pointing vector
2. Determine geographic launch vector
3. Perform ray trace
4. Reduce to vessel reference point.

Presented with new surface or watercolumn sound speed information in post-processing, the procedure varies only in the entry point of the four-step process above. Three scenarios exist with the entry point for each case summarised in Table 1, with each step discussed further below.

Vessel Coordinate System

Before proceeding, it is necessary to discuss the vessel coordinate system and rotation matrices that are used in this work. The coordinate system used throughout is right-handed with the positive x-axis pointing towards the bow, the positive y-axis pointing towards starboard and the positive z-axis pointing below the
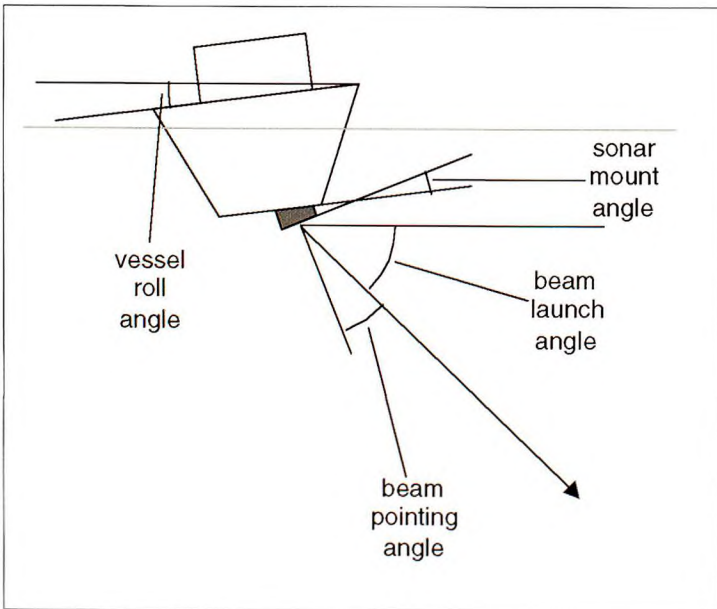

Figure 3: Illustration of the difference between beam-pointing angle and beam launch angle. The beam-pointing angle is relative to the transducer boresite whereas the beam launch angle is referenced to the local vertical and accounts for effects due to vessel orientation and mount angles. Note that pitch and yaw are ignored in this illustration though they play a potentially significant role in the determination of beam launch angle. The beam-pointing angle is corrected during the beam re-pointing procedure outlined in this work.

vessel. The sign convention for angular measurements follows the right hand rule, i.e. positive roll is to starboard (starboard sinks, port rises), positive pitch is nose-up (bow rises, stern sinks), and positive yaw is clockwise (bow turns to starboard). The rotations of roll (θ), pitch (ϕ) and yaw (γ) about the x, y, and z-axes described earlier are expressed by the following matrices, as can be found in any linear algebra text:

$$R(\theta) = \begin{bmatrix} 1 & 0 & 0 \\ 0 & \cos\theta & -\sin\theta \\ 0 & \sin\theta & \cos\theta \end{bmatrix} R(\phi) = \begin{bmatrix} \cos\phi & 0 & \sin\phi \\ 0 & 1 & 0 \\ -\sin\phi & 0 & \cos\phi \end{bmatrix} R(\gamma) = \begin{bmatrix} \cos\gamma & -\sin\gamma & 0 \\ \sin\gamma & \cos\gamma & 0 \\ 0 & 0 & 1 \end{bmatrix}$$

The rotation is applied via matrix multiplication of the matrix and vector, with subsequent rotations applied in a right-to-left manner, for example, to apply a roll, pitch and yaw rotation, one multiplies in the order shown in (1).

$$\vec{V}_{rotated} = R(\gamma) \cdot R(\phi) \cdot R(\theta) \cdot \vec{V}_{original} \tag{1}$$

The rotation matrices can be pre-multiplied, giving a single rotation matrix that encompasses the effect of all three individual rotations (ensuring that the same multiplication order is respected). Doing so gives the following rotation matrix; this is the general rotation matrix that is used throughout this work.

$$R_{\theta\phi\gamma} = \begin{bmatrix} \cos\phi \cdot \cos\gamma & \sin\theta \cdot \sin\phi \cdot \cos\gamma - \cos\theta \cdot \sin\gamma & \cos\theta \cdot \sin\phi \cdot \cos\gamma + \sin\theta \cdot \sin\gamma \\ \cos\phi \cdot \sin\gamma & \sin\theta \cdot \sin\phi \cdot \sin\gamma + \cos\theta \cdot \cos\gamma & \cos\theta \cdot \sin\phi \cdot \sin\gamma - \sin\theta \cdot \cos\gamma \\ -\sin\phi & \sin\theta \cdot \cos\phi & \cos\theta \cdot \cos\phi \end{bmatrix}$$

Step 1: Re-compute Beam Pointing Vector

Multibeam sonars rely on the principle of electronic beam steering to direct the Main Response Axis (MRA) of the transmitter and/or receiver arrays. Both arrays typically consist of a series of acoustic elements, with the signals from all elements being summed to focus the response pattern of the array into a narrow beam. Beam steering, or the redirection of the MRA, is achieved through the addition of time or phase delays during the element summation process; beam steering requires knowledge of the speed of sound at the array face since phase and time delays are based upon the wavelength associated with the sonar's operating frequency.
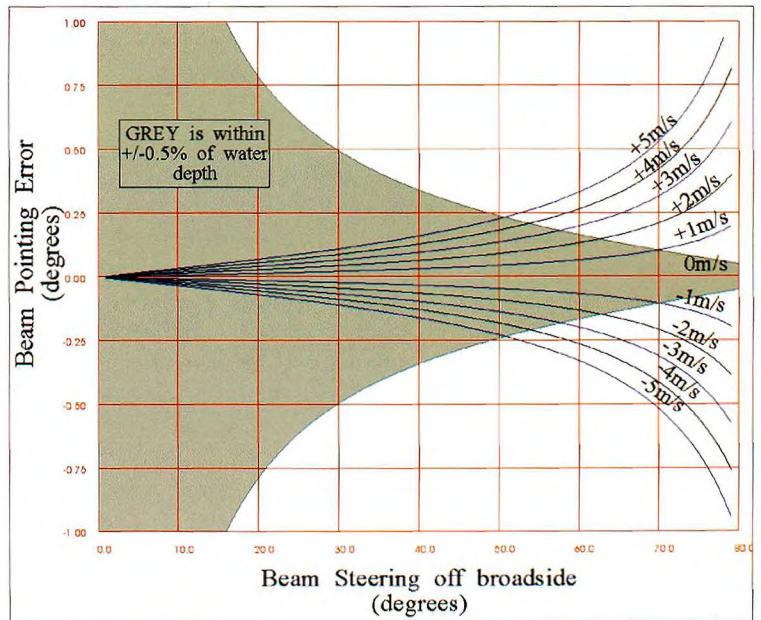

Figure 4: Linear array beam steering sensitivity to surface sound speed error [after Hughes Clarke, 2003a]. Clearly, even small errors in surface sound speed can degrade the accuracy of depth solutions associated with outer beams.

Errors in the knowledge of surface sound speed lead directly to systematic errors in beam pointing angles through the calculation of wavelength based on sound speed. These errors grow proportionally to steering angle (though non-linearly), thus the largest error is encountered in the most steered beams of a steered linear array whereas the accuracy of beams near broadside suffers little, as shown in Figure 4. The *Amundsen*'s EM300 is installed nearly level, as such, the major issues occur at angles away from nadir. This is not the case for tilted line arrays (e.g. EM3000D or EM12D, etc).

Errors due to imperfect surface sound speed are most easily observed during large vessel roll events since they introduce a variable non-linear tilting of the swath that correlates with receiver roll [Hughes Clarke, 2003b]. The *Amundsen*'s EM300 installation produces a signature artifact in the face of surface sound speed errors since the receiver array is mounted approximately 6° from level. In order to maintain a symmetric receiver sector, for example +/-60°, the transceiver must steer the outer beams on the starboard side 66° whereas the port beams need only be steered to 54°. As such, errors in surface sound speed generate a distinctive non-linear tilt to the swaths, as shown by the black soundings in Figure 5.

Procedure & Application
Re-pointing a beam involves computing a new array-relative steering angle based on the new sound speed and original steering angle and sound speed. Snell's Law relates the four values:

$$\frac{c_1}{\sin \theta_1} = \frac{c_2}{\sin \theta_2} \tag{2}$$

Given sound speeds c_1 and c_2 and the original array-relative steering angle θ_1, we solve for the new steering angle as such:

$$\theta_2 = \sin^{-1}\left(\frac{c_2}{c_1} \cdot \sin \theta_1 \right) \tag{3}$$

Step 2: Determine Geographic Launch Vector
In general, fourteen angles are required to determine a sounding's geographic pointing vector, consisting of four roll, pitch and heading triplets and two steering angles [Hughes Clarke, 2003a]:
(1) Orientations at time of transmit and receive (6 angles)
(2) Transmitter and receiver mounting angles (6 angles)
(3) Steering angle on transmit and receive (2 angles).
The orientations at the moments of transmit and receive are ascertained by determining the times of both events and then interpolating the orientation using the vessel attitude time-series values before and after each time. The transmit time is recorded with the bathymetry packet whereas the receive time is computed through the addition of the transmit time and the two-way travel-time for each receive beam. The mount angles are determined during a patch test or vessel installation survey. It is important to note that some sonars share the same mount angles for the transmitter and receiver as they are installed as a single physical unit (and assuming perfect orientation within the transducer). Others, particularly the larger arrays, have independently installed transmitters and receivers that need be neither orthogonal nor coplanar and thus one needs separate mount angles for each.
Given the necessary angular measurements, the first step is to determine the transmitter and receiver directional vectors at the time of transmit and receive. These vectors are then used to build a coordinate system from which the beam's pointing vector can be determined using the transmit and receive steering angles; this vector is then referenced to the local level coordinate system. The procedure begins with an ideal transmit unit vector pointing perfectly along the ship's x-axis, i.e. (1,0,0), with the ship being perfectly level and facing north. This ideal vector is then rotated using the transmitter alignment angles, immediately followed by the orientation of the transmitter at transmit time, as in (4). The same is done in (5) for the receiver with its mount angles and orientation; however, the ideal receiver vector is oriented perfectly with the ship's y-axis, i.e. (0,1,0). Note that the rotation matrices in (4) and (5) are composed of three individual rotation matrices that represent roll, pitch, and heading.

$$\overrightarrow{TX} = R_{orientation} \cdot R_{alignment} \cdot \overrightarrow{TX}_{ideal} \tag{4}$$

$$\overrightarrow{RX} = R_{orientation} \cdot R_{alignment} \cdot \overrightarrow{RX}_{ideal} \tag{5}$$

The vectors *TX* and *RX* represent the orientation of the transmitter and receiver at the times of transmit and receive, respectively, in the locally level coordinate system. Figure 6 demonstrates how these two vectors are then used to build a coordinate system in which the beam-pointing vector can be measured. This coordinate system, referred to as the primed coordinate system, is created through the use of the cross product:

$$\overrightarrow{X'} = \overrightarrow{TX} \tag{6}$$

$$\overrightarrow{Z'} = \overrightarrow{TX} \times \overrightarrow{RX} \tag{7}$$

$$\overrightarrow{Y'} = \overrightarrow{Z'} \times \overrightarrow{X'} \tag{8}$$

The beam-pointing vector is then computed in the primed coordinate system through the following equations, as depicted in Figure 7:

$$\delta = \cos^{-1}(\overrightarrow{TX} \cdot \overrightarrow{RX}) - \frac{\pi}{2} \tag{9}$$

$$y_1 = \frac{-\sin(RX_{steer})}{\cos(\delta)} \tag{10}$$

$$y_2 = \sin(TX_{steer}) \cdot \tan(\delta) \tag{11}$$

$$radial = \sqrt{(y_1 + y_2)^2 + \sin^2(TX_{steer})} \tag{12}$$

$$x = \sin(TX_{steer}) \tag{13}$$

$$y = y_1 + y_2 \tag{14}$$

$$z = \sqrt{1 - radial^2} \tag{15}$$

$$\overrightarrow{BV}_{prime} = \begin{bmatrix} x \\ y \\ z \end{bmatrix} \tag{16}$$

The beam-pointing vector is then rotated into the ideal geographic coordinate system with a rotation matrix that describes the transformation between the ideal and primed coordinate system. In general, a matrix describing the axis rotation required to change perspective from one coordinate system to another can be constructed via (17). Recall that idealised unit vectors (<1,0,0>, <0,1,0>, <0,0,1>) were used to construct the geographic coordinate system, thus each of the inner products in the matrix elements of (17) reduce to a single value of the axes in the primed coordinate system:

$$R_{Geo} = \begin{bmatrix} \overrightarrow{X} \cdot \overrightarrow{X'} & \overrightarrow{Y} \cdot \overrightarrow{X'} & \overrightarrow{Z} \cdot \overrightarrow{X'} \\ \overrightarrow{X} \cdot \overrightarrow{Y'} & \overrightarrow{Y} \cdot \overrightarrow{Y'} & \overrightarrow{Z} \cdot \overrightarrow{Y'} \\ \overrightarrow{X} \cdot \overrightarrow{Z'} & \overrightarrow{Y} \cdot \overrightarrow{Z'} & \overrightarrow{Z} \cdot \overrightarrow{Z'} \end{bmatrix} = \begin{bmatrix} \overrightarrow{X'}_x & \overrightarrow{Y'}_x & \overrightarrow{Z'}_x \\ \overrightarrow{X'}_y & \overrightarrow{Y'}_y & \overrightarrow{Z'}_y \\ \overrightarrow{X'}_z & \overrightarrow{Y'}_z & \overrightarrow{Z'}_z \end{bmatrix} \tag{17}$$
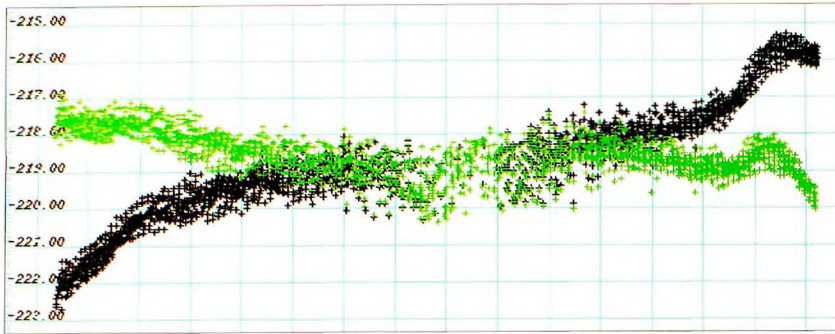
Figure 5: Example of surface sound speed artifacts from several swaths of data observed with CCGS Amundsen (surface sound speed error is approximately 50m/s). Horizontal boxes are 25 metres, black and green symbols represent raw and corrected soundings.

Note the curl on the starboard outermost side of the swaths (which have to have extra steering to account for the 6° receiver mounting to port); it is thought that this artifact is due to beam steering errors arising from the titanium-polymer ice windows installed over the receiver to protect the transducers during ice breaking.

The rotation matrix in (17) is then used to transform the elements of the beam vector in the primed coordinate system to the geographic coordinate system:

$$\overrightarrow{BV} = R_{Geo} \cdot \overrightarrow{BV}_{prime} \tag{18}$$

The beam depression angle and azimuth are then computed in the usual manner:

$$\alpha = \tan^{-1}\left(\frac{\overrightarrow{BV}_X}{\overrightarrow{BV}_Y}\right) \tag{19}$$

$$\beta = \tan^{-1}\left(\frac{\overrightarrow{BV}_Z}{\sqrt{\overrightarrow{BV}_X^2 + \overrightarrow{BV}_Y^2}}\right) \tag{20}$$

Finally, the azimuth is reduced to that of the heading at time of transmit.

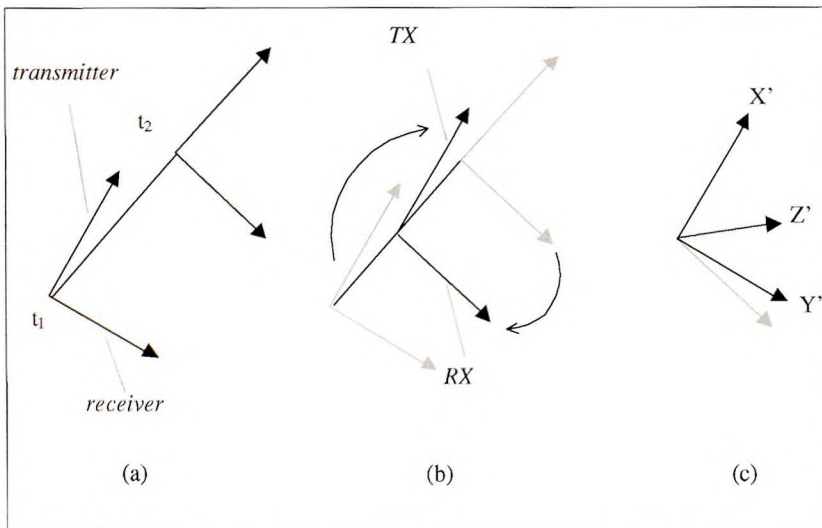$$\alpha_{relative} = \alpha - \alpha_{ship} \tag{21}$$

Figure 6: Construction of primed coordinate system. The orientation of the transmitter/ receiver assembly changes from the time of transmit and receive, represented by t_1 and t_2, respectively, in (a). The transmit vector (TX) and the receiver vector (RX) are then migrated to the midpoint between the two positions, as in (b). A coordinate system is then built in which TX is the X' axis, the Z' axis is orthogonal to the plane containing TX and RX and the Y' axis is orthogonal to the X' axis and Z' axis (depicted in (c)). It is in this coordinate system that the beam-pointing vector is computed.
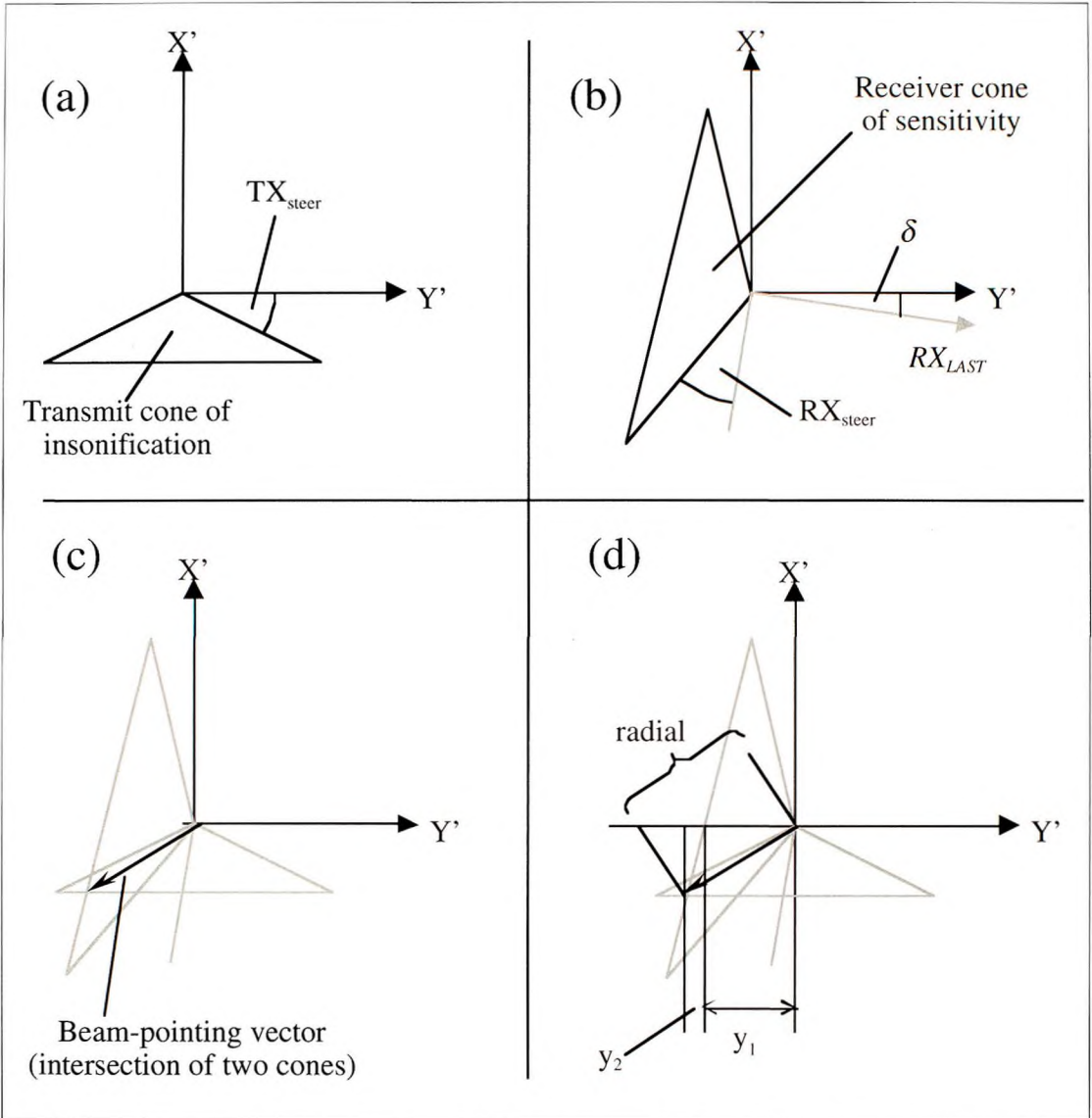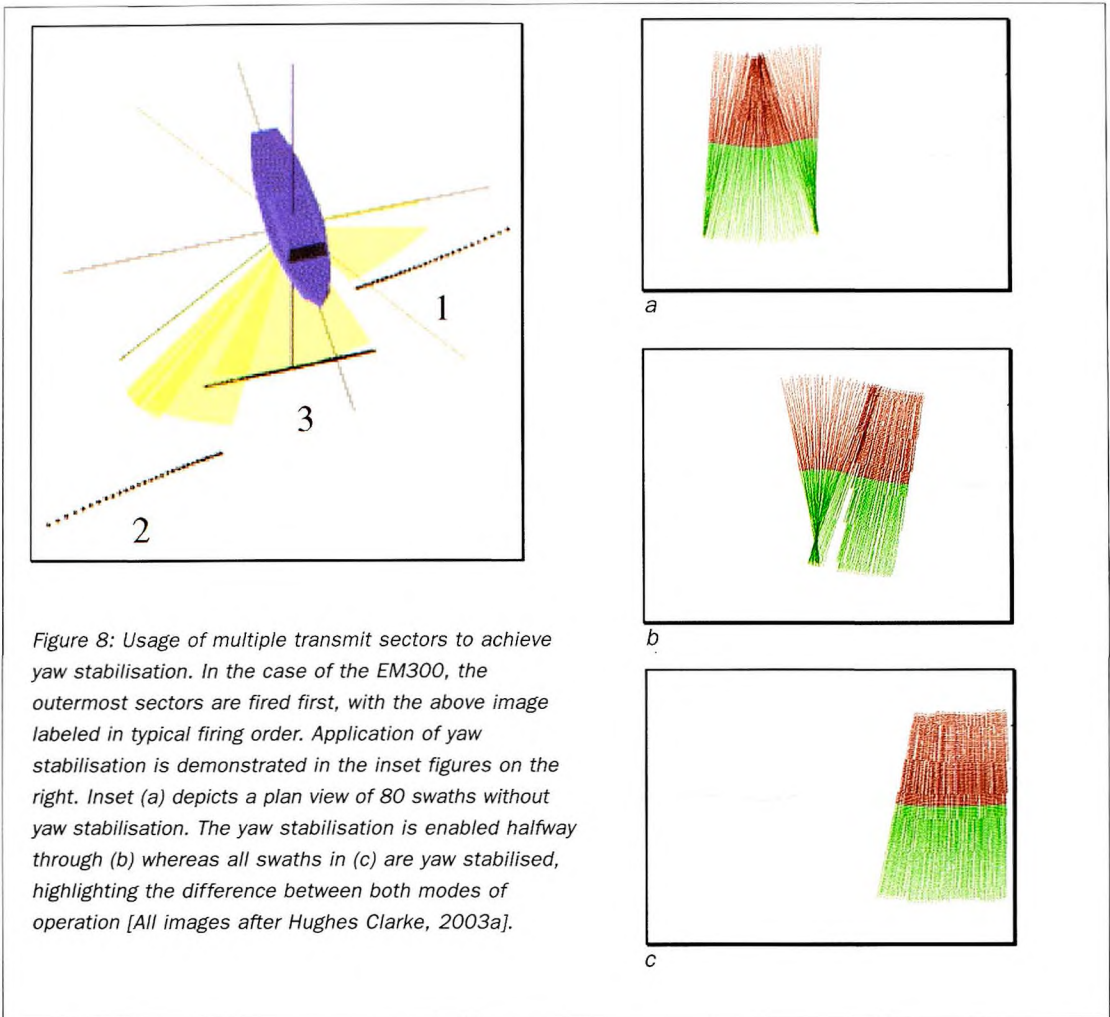
Figure 7: Geometry of transmit and receiver cone intersection. The beam-pointing vector lies on the intersection of the transmitter cone of insonification and the receiver cone of sensitivity, shown in (a) and (b) respectively with the intersection shown in (c). Image (d) demonstrates the geometry used to derive the beam-pointing vector coordinates.

Complications

The process becomes difficult at this point for the EM300 as installed on the *Amundsen* due to the multi-sector transmitter arrangement that allows it to stabilise the transmit pattern for yaw, as shown in Figure 8. Multiple transmit sectors complicate the beam pointing vector determination in two ways: (1) each transmit sector has a unique transmit time, orientation and steering angle, and (2) the receive times are relative to the transmit time, so each receive beam must be associated with a unique transmit sector.

The EM300 features several operational modes, each geared to a different range of water depths. The deepest mode features a long pulse length and low number of transmit sectors (due to signal extinction in the outer sectors) while the shallow modes use shorter pulse lengths [Kongsberg Simrad, n.d.]. The pertinent information for each mode is summarised in Table 2 below. Note that the sector boundaries and

Figure 8: Usage of multiple transmit sectors to achieve yaw stabilisation. In the case of the EM300, the outermost sectors are fired first, with the above image labeled in typical firing order. Application of yaw stabilisation is demonstrated in the inset figures on the right. Inset (a) depicts a plan view of 80 swaths without yaw stabilisation. The yaw stabilisation is enabled halfway through (b) whereas all swaths in (c) are yaw stabilised, highlighting the difference between both modes of operation [All images after Hughes Clarke, 2003a].

sector firing intervals were provided from the Kongsberg Simrad engineer who was onboard during the transit (it should be noted that as of early 2004, new Simrad datagram formats supply all of the required information). Personal communications with Kongsberg Simrad have confirmed the sector firing order to be outermost port sector, then outermost starboard, and so on, until the central sector is reached (as demonstrated in Figure 8).

Mode	Number of Sectors	Sector Boundaries (degrees) positive=port, negative=starboard	Sector Firing Interval (ms)
Extra-Deep	3	10.5°, -10.5°	15.51
Very-Deep	9	44.0°,31.5°,20.5°,10.5° -10.0°, -21.0°, -31.5°, -44.0°	5.32
Deep	9	63.4°, 44.7°, 29.5°, 18.4°, -17.0°, -31.0°, -44.7°, -63.5°	5.32
Medium	3	60.0°, -60.0°	2.66
Shallow	3	60.0°, -60.0°	1.11
Very-Shallow	3	60.0°, -60.0°	1.11

Table 2: EM300 operational modes.

To perform a beam re-pointing using data from the EM300, one must first determine the operational mode (stored in the run-time telegram, output by the transceiver). The operational mode implies the number of sectors, in addition to the angular boundaries and time offsets between them. These values are then used to determine the times and orientations at time of transmit and receive. The procedure is as such:

1. For any given receive beam, one must determine its associated transmit sector using the original estimate of depression angle stored in the depth telegram

2. Determine the transmit time of the first sector (the time stamp of the depth telegram), then add the appropriate number of sector firing intervals to arrive at the transmit time of the receive beam's transmit sector. For example, referring to Figure 8, the third sector in Extra-Deep mode would be fired 30.02ms after the first sector (2 x 15.51ms = 30.02ms). This offset is added to the depth telegram time stamp to arrive at the transmit time of the sector in question

3. Compute the receive time by adding the receive beam's two-way travel time to the sector's transmit time

4. Use the transmit and receive times to look up the orientation for both events and proceed as outlined in the procedure above.

Step 3: Perform Ray trace

Ray tracing algorithms allow for the modeling of the effect of refraction of a ray path given an initial launch angle, transducer depth and sound speed profile. Details of ray tracing techniques are available in most oceanographic texts (e.g. Medwin and Clay, (1998)), the discussion herein is as such limited to the computation of the input parameters to a ray tracing algorithm, namely the transducer depth.

If significant along or across track lever arms exist between the vessel's center of mass and the sonar, then the transducer draft is subjected to an induced heave when the ship pitches and/or rolls (in addition to the heave measured by the motion sensor). The induced heave may be accounted for by rotating the transducer's lever arms with the roll and pitch and using the resulting z component of the rotated vector (assuming that the reference point is at or near the center of mass of the vessel (or at least the heave output is described for that location); this begins by rotating the lever-arms by a rotation matrix constructed using the orientation at the time of transmit, as in (22).

$$\overrightarrow{TX}_{rotated} = R_{orientation} \cdot \overrightarrow{TX}_{offsets} \tag{22}$$

The z-ordinate of the waterline and the heave at transmit are then applied to the z-ordinate of the rotated lever-arm vector, as in (23). This yields the actual vertical displacement between the reference point and the sonar.

$$draft_{TX} = Z_{TX_{rotated}} - Z_{waterline} + heave_{TX} \tag{23}$$

The same procedure is carried out for the receiver using its lever arms at orientation at the time of reception. The mean of the two computed drafts is then used as the starting point for the ray trace, along with the depression angle computed in (20).

The ray tracing proceeds as usual, with one exception: the surface sound speed is introduced at the transducer depth as a 'snapback' layer to allow for the preservation of Snell's constant at the transducer face, as discussed by Cartwright and Hughes Clarke (2002). Assuming that the variation in the profiles exists mainly in the top portion of the water column (as was usually the case with the 2003 dataset), the true and computed ray paths will become parallel once the variable surface layer is passed. This is due to the fact that the ray parameter, or Snell's constant, will maintain the correct departure angle at the deepest portion of the layer of surface variability regardless of the intervening sound speed structure in the water column. An error in depth and across-track distance is introduced due to the outdated water column, however, this error is constant and becomes increasingly insignificant with depth, especially in the case where the thickness of the variable surface layer is small with respect to the entire water column [Cartwright, 2002].

Step 4: Reduce to Vessel Reference Point

The output of the ray trace is the total horizontal and vertical distance traveled during the ray's flight through the watercolumn in a vertical plane lying along the ship-referenced heading computed in (21). The vertical distance is added to the mean draft to yield the depth measurement (which need only be corrected for tide). The horizontal distance is broken into along-track and across-track components using the beam azimuth as derived during the cone intersection described earlier, as shown in (24) and (25).

$$across = d_{horizontal} \cdot \sin(\alpha_{relative}) \tag{24}$$

$$along = d_{horizontal} \cdot \cos(\alpha_{relative}) \tag{25}$$

The rotated transmitter lever-arms computed in (22) are added to these components in order to reference the sounding to the origin of the ship's coordinate system at the time of transmit.

Practical Application: EM300

The above methodology was applied to a subset of the soundings collected during the 2003 transit. Statistical analysis of the application of surface sound speed is not possible due to a lack of overlapping survey lines. As such, accuracy checks are limited to the comparison of soundings from swaths preceding and following the application of a beam pointing-angle correction.

The sound speed artifacts shown in Figure 2 can be categorised based on their causes: either (1) the surface sound speed pump had failed, or (2) the pump was functioning, but its readings were ignored. Table 3 summarises the required action in post-processing. Each of these cases is discussed further below.
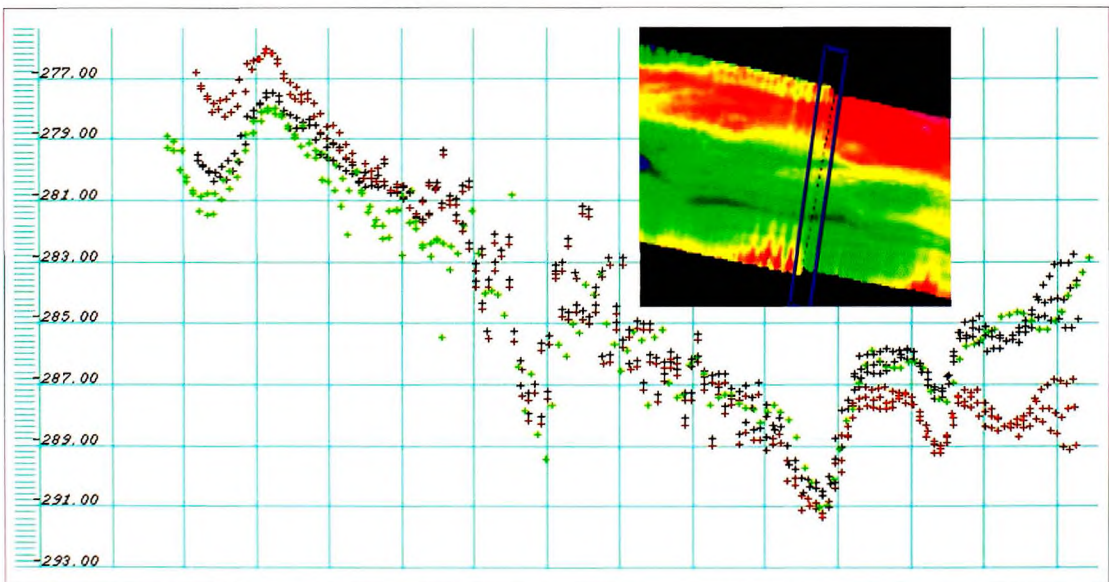

Figure 9: Across-track profile of raw and corrected data in Section B, bordering a transition from profile-based to probe-based surface sound speeds. Soundings are from three across-track profiles from the two survey lines bordering the transition (as shown in the inset colour coded depth image, ship track is from right to left). Green soundings are from the survey line collected after the probe was enabled, while the red and black soundings represent the raw and corrected soundings, respectively, from the preceding survey line where the probe was disabled. Note that the corrected soundings (black) agree well with the trend of the profile collected immediately after the probe was enabled (green). Horizontal boxes are 100 metres wide.

Artifact	Solution
A	Linearly interpolate surface sound speed from 1454 m/s to 1450 m/s, based on nearest valid data.
B	Linearly interpolate surface sound speed from 1435 m/s to 1432 m/s, based on nearest valid data.
C	Use logged surface sound speed value.
D	Use estimate of 1433 m/s based on nearest valid data.
E	Use logged surface sound speed value.
F	Use logged surface sound speed value.

Table 3: Proposed solutions for observed sound speed artifacts.

Re-pointing Based on Estimates of Correct Surface Sound Speed

Sections A, B, and D fall within the category of soundings that must be corrected with estimates of surface sound speed. In the case of A and B, the operators noticed the failure and the last sound speed profile was used as the source of sound speed for beam steering purposes (the transceiver estimates the transducer's vertical position in the watercolumn and interpolates a sound speed value from a sound speed profile). Case D arose from an unnoticed pump failure, with the sound speed probe supplying the transceiver with grossly erroneous values. In post-processing, there was no choice but to re-point the beams based on an estimate of the correct surface sound speed for all three cases. Selected results are shown using data from Sections B and D.
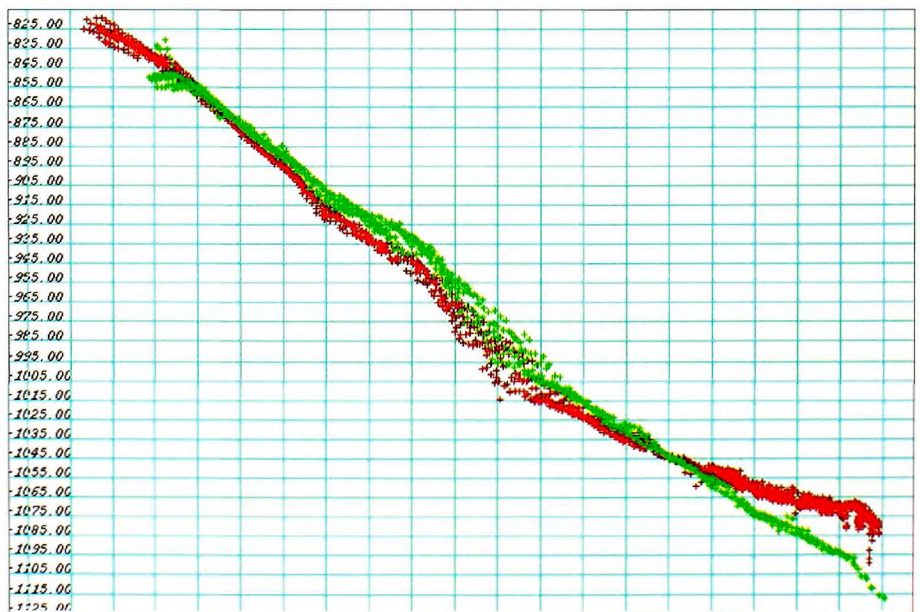
Section B

Data from the surface sound probe became unusable due to heavy icebreaking, thus the probe was disabled and the transceiver was configured to use the sound speed from the last sound speed profile. Data collected immediately before reactivation of the probe were re-pointed using an estimated surface sound speed of 1431.9m/s (instead of 1454.4m/s). Across-track plots of the soundings before and after the transition back to using the probe are shown in Figure 9.

Section D

Data collected in Section D are characterised by a gross error in surface sound speed since the failure of the probe went unnoticed overnight with the probe reporting values of approximately 1480m/s (where-

Figure 10: Raw soundings of Section E (green) compared to soundings from overlap line collected prior to sensor failure (red). Error approaches 1.4% of water depth in outer beams on right side of figure. Horizontal boxes are 150 metres wide.
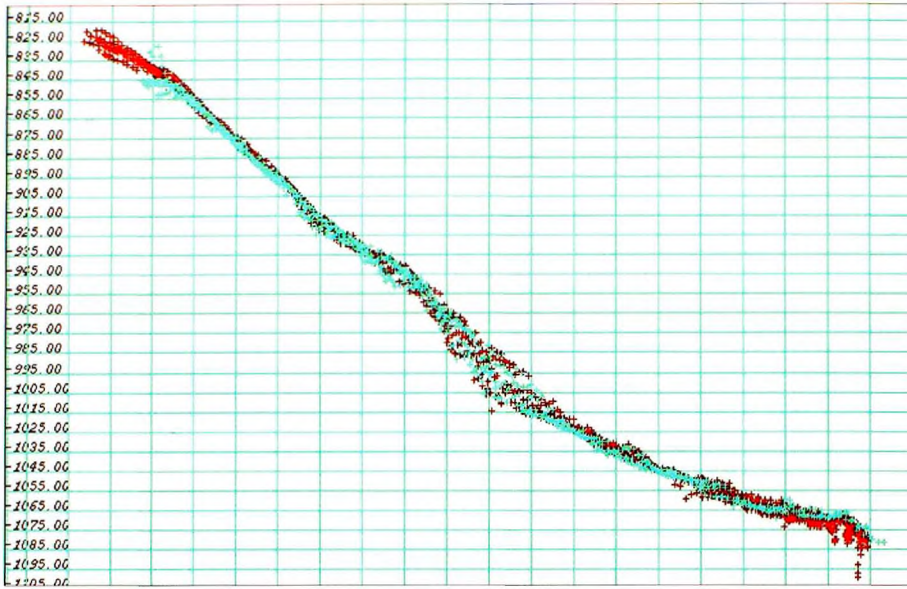
Figure 11:
Corrected
soundings (blue)
of Section E
compared to
soundings from
overlap line
collected prior to
sensor failure
(red). Horizontal
boxes are 150
metres wide.

as the true value was closer to 1430m/s). Fortunately, a small area of overlap was found between lines collected before and after the probe failure. Subsets of the raw and corrected soundings are shown in figures 10 and 11, respectively.

Re-pointing Using Sound Speed Probe Data

Sections C, E, and F are incorrect because the surface sound speed probe values were ignored, either accidentally or intentionally, in favour of the value provided from the last sound speed profile (the grey arrows in Figure 12 indicate the sound speed profile value that was used instead of the value measured by the probe). Fortunately, the EM300 raw data format logs the surface sound speed probe values even if they are not applied. The data recorded during these periods are graphed in Figure 12; these values can clearly be used to correct the soundings in these sections. A subset of the data from Section F is presented.

Section F

In this case, the operator momentarily toggled between using the probe and the last profile as the source of sound speed for beam steering. After a brief interlude of using the profile as the source, the operator switched back to using the probe. The soundings during this time period must be corrected based on the logged probe values since a surface sound speed error of approximately 11m/s was introduced during this short time (introducing a depth error of approximately 1.25% of water

depth in the outer beams). The transition between probe sound speed and profile sound speed is shown in Figure 13, with the raw and corrected soundings contrasted against the ping immediately preceding the transition.

Conclusion and Recommendations

It has been demonstrated that it is possible to correct soundings corrupted by incorrect surface sound speed values in post-processing using the technique outlined in this document as long as the following information are retained:
1. Array relative steering angles
2. Two way travel times to bottom detection
3. Full resolution orientation time series
4. Lever arms between all sensors, and alignment angles
5. Sound speed applied in beam steering process.
Several instances of faulty surface sound speed were re-processed with promising results, even in the face of gross sound speed errors applied by the transceiver. This technique can be extended to other sonars which store the above information in their data format and whose operation is well understood. Complications due to multiple transmit sectors, including inter-sector firing boundaries and firing intervals, must be resolved before the procedure outlined herein can be applied.

Given the transit conditions under which the data were collected, it is difficult to test the robustness of

Figure 12: Comparison of applied sound speed vs. recorded sound speed. Applied values are shown in blue, recorded values are in green. Red samples are taken from transducer depth in sound speed profiles. Sections C, E, and F can be corrected using the actual recorded values.
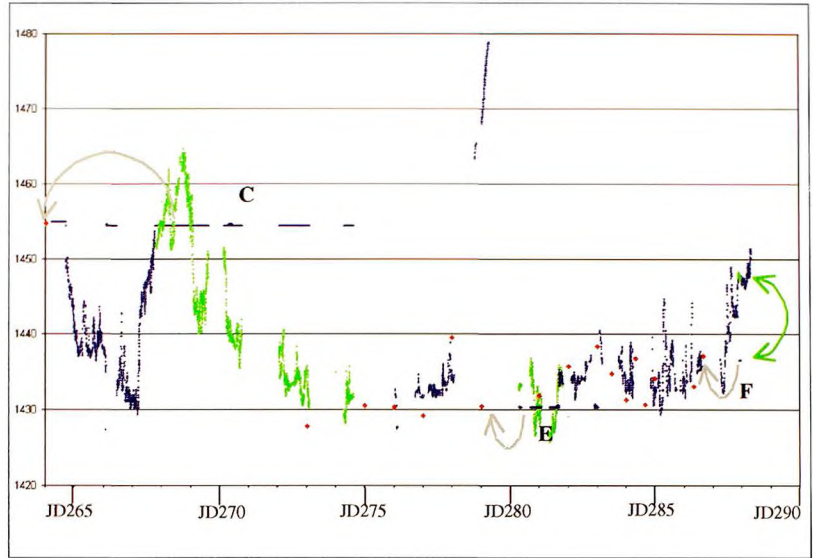
the method presented in this work. A rigorous testing exercise should be planned in which a small patch is surveyed (with the sound probe enabled) to generate a reference surface. Cross-lines can then be run with intentionally incorrect surface sound speed values being entered into the system to observe the effect and to test the robustness of the procedure used in

this work. Though not explicitly mentioned in the text, the offsets between the transmitter and receiver have been ignored. While the errors incurred are negligible in deep water, future work should focus on modeling the intersection of non-concentric cones such that the model more correctly represents reality in the case of shallow water soundings.
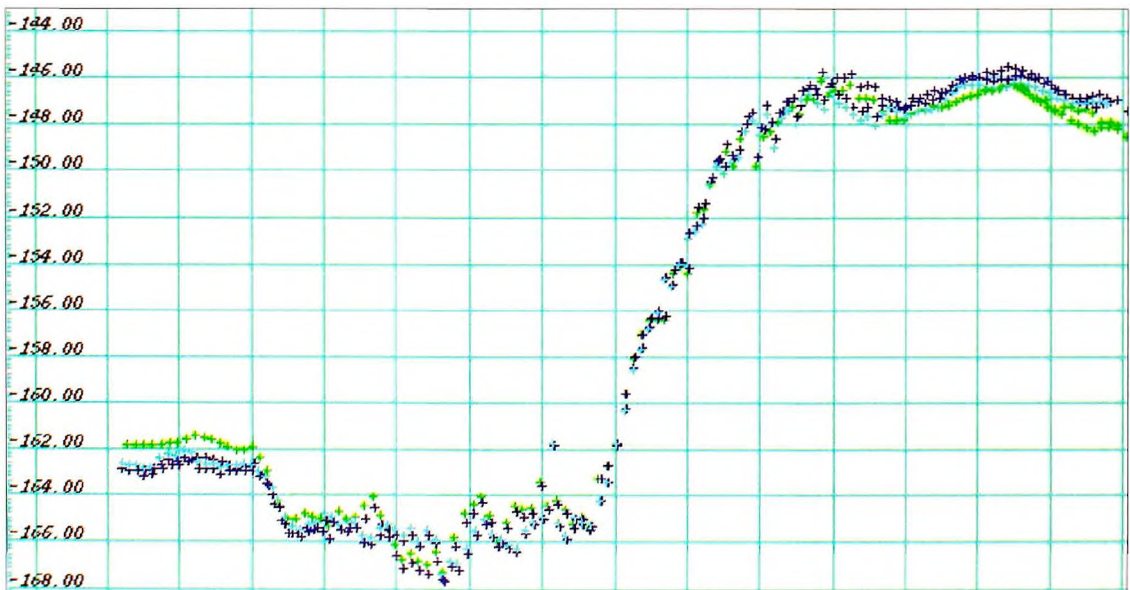

Figure 13: Re-pointing soundings in Section F. Data are from 2 swaths surrounding the transition from probe to profile as the source of sound speed for beam steering. Soundings in light blue were collected prior to the transition and are considered correct. Green soundings were collected using the erroneous sound speed value from the profile with the dark blue soundings being the corrected versions of the green. The re-pointing procedure has removed depth errors of 1.25% of water depth in the outer beams of the green soundings. Horizontal boxes are 25 metres wide.

Acknowledgements

References

Beaudoin, J.D., Hughes Clarke, J.E. and J.E. Bartlett (2004). Retracing (and re-raytracing) Amundsen's Journey through the Northwest Passage. *Canadian Hydrographic Conference 2004, Proceedings*, CDROM

Cartwright, D.S. and J.E. Hughes Clarke (2002). Multibeam Surveys on the Fraser River Delta, Coping with an Extreme Refraction Environment. *Canadian Hydrographic Conference 2002, Proceedings*, CDROM

Hughes Clarke, J.E., M. Lamplugh and E. Kammerer (2000). Integration of near-continuous sound speed profile information. *Canadian Hydrographic Conference 2000, Proceedings*, CDROM

Hughes Clarke, J.E. (2003a). GGE 3353 Lecture Notes. Department of Geodesy and Geomatics Engineering, University of New Brunswick, Fredericton, New Brunswick

Hughes Clarke, J.E. (2003b). Dynamic Motion Residuals in Swath Sonar Data: Ironing out the Creases. *International Hydrographic Review*. v. 4, no.1, p. 6-23

Kongsberg Simrad (n.d.). Simrad EM300 Multibeam Echo Sounder. Product Specification, Horten, Norway

Medwin, H. and C.S. Clay, (1998). *Acoustical Oceanography*, Academic Press, San Diego

Biographies

Jonathan Beaudoin is a graduate student studying at the University of New Brunswick in Fredericton, New Brunswick, with his main research interest being acoustic imagery calibration for RESON multibeam echosounders. In addition to being a student, Jonathan is the Ocean Mapping Group's dedicated research assistant associated with the ArcticNet project, which sees him involved in all stages of arctic mapping operations. His background in Computer Science and Geomatics Engineering is put to good use through involvement in post-processing software design in virtually all fields of research currently being pursued by the Ocean Mapping Group.

John Hughes Clarke is the Chair of Ocean Mapping at the University of New Brunswick. He has 20 years experience working with swath sonar systems. He has degrees in geology and oceanography from Oxford, Southampton and Dalhousie and has been a post-doc at BIO and at James Cook University (Queensland). He has been at UNB for 13 years, working with and now leading the Ocean Mapping Group.

Jason Bartlett is a graduate of the Geodesy and Geomatics Engineering program at the University of New Brunswick. He is currently employed with the Canadian Hydrographic Service and works in close cooperation with the Ocean Mapping Group onboard the CCGS *Amundsen*. He has experience in both seismic surveying and hydrography which are both integral to the work onboard the CCGS *Amundsen*.

E-mail: jonnyb@omg.unb.ca